A composite structure for efficient photocatalysts: anatase nanocrystals attached to exfoliated clay layers

Xuzhuang Yang [a,d], Huaiyong Zhu [a*], Jiangwen Liu [a], Xueping Gao [b], Wayde N. Martens [a], Ray L. Frost[a], Yuenian Shen [c], Zhangfu Yuan [d 1]

Abstract: It is believed that increasing the content of anatase nanocrystals and improving the accessibility of these crystals to reactants (UV photons, organic contaminant molecules and oxygen molecules) will enhance photocatalytic performance. Thus we designed the synthesis approach to achieve such structures. The synthesis involves reaction of clay suspensions with $TiOSO_4$, which leads to formation of anatase nanocrystals attaching to clay layers through Ti-O-Si bonds. The influence of the experimental parameters on the structure of the final photocatalysts is investigated. It is found that the crystal size, the pore size and the specific surface area of the catalysts, can be tailored by manipulating the acidity, the ratio of Ti/clay and the hydrothermal temperature of the synthesis systems. Such a synthesis is different from the conventional approach of pillared intercalated layered clays. The activity of these catalysts for the degradation of phenol

[a] Dr X. Z. Yang, A/Prof. H. Y. Zhu, Dr J. W. Liu Dr W. N. Martens, Prof. R. L. Frost, Inorganic Materials Research Program, School of Physical and Chemical Sciences, Queensland University of Technology, GPO Box 2434, Brisbane, QLD 4001 Australia, Fax: 61 7 3864 1581, Email: hy.zhu@qut.edu.au. Current address of Dr X. Z. Yang is College of Chemistry and Chemical Engineering, Inner Mongolia University, Huhhot, 010021, China.

[b] Prof X. P. Gao, Institute of New Energy Material Chemistry, Nankai University, Tianjin 300071, China.

[c] Prof Y. N. Shen, College of Chemistry and Chemical Engineering, Inner Mongolia University, Huhhot, 010021, China.

[d] Prof. Z. F. Yuan Institute of Process Engineering, The Chinese Academy of Science, Beijing 100080, China

was investigated, proved far better than titania pillared clays by conventional synthesis.

Keywords: photocatalysis . exfoliated layered clay . beidellite . titania . phenol

Introduction

Anatase is regarded as the most active TiO_2 polymorph for decomposing recalcitrant organic pollutants in water and air under ultraviolet (UV) irradiation.[1-3] It is non-toxic, relatively inexpensive, chemically stable throughout a wide pH range and robust under UV illumination. It can be used in various processes such as odor elimination from drinking water, degradation of oil spills in surface water systems and degradation of toxic organic contaminants like herbicides, pesticides and highly coloured dyes. The photo-catalytic reaction takes place on anatase surfaces so that the catalysts of ultra-fine anatase powders with a particle size at a scale of tens of nanometers should exhibit a superior activity because of the large specific surface. However, ultra-fine powders have a strong tendency to agglomerate into larger particles, resulting in an adverse effect on catalyst performance. Furthermore, it is very hard to recover the powders after the reaction, leading to a potential difficulty in downstream separation.[4,5] Continuing efforts have been made to develop alternate approaches to fabricate the structures which can be separated readily, and have the superior performance of anatase nanocrystals.

To achieve anatase structures with a large surface area, introducing a second component to partition the fine anatase particles is a feasible option. Actually, layered clays intercalated with TiO_2 particles (the pillars), TiO_2-pillared clays,[6-16] developed by Sterte [17] and Yamanaka et al [18] is a composite structure with a relative large TiO_2 surface area. The clay layers are about 1 nm thick and carry negative charges.[19, 20] There are charge-balancing cations between the layers.

Positive charged sol particles of titanium hydrate, prepared by hydrolysis of a titanium compound, can replace the interlayer cations by an ion exchange process.[17, 18] They are converted to oxide pillars after being heated to above 500^{o}C, propping apart the clay layers apart. The lateral dimension of the clay layer is between hundreds of nanometers and several microns, so that the TiO_2-pillared clay particles can be readily separated out after the photocatalytic reaction. However, there are inherent structural problems in TiO_2-pillared clays, which seriously limit their applications. First, the TiO_2 pillars are small (< 2 nm) and generally amorphous particles.[21] An anatase form of TiO_2 is necessary for an efficient photocatalyst.[1-3] The TiO_2 pillars in the TiO_2 pillared clays, however, are too small to form crystallites. Second, the pore size of these pillared clays, which is associated with the pillar size, is too small to allow the large organic molecules to diffuse quickly to the surface of anatase pillars. It is extremely difficult to obtain large pillar precursors without precipitation in the conventional pillaring process. The poor activity of amorphous TiO_2 pillars and the diffusion difficulty make the TiO_2 pillared clays exhibit a moderate catalytic performance for photodegradation of organic pollutants which are usually large molecules.[22]

To pursue efficient photocatalysts, in the present study, we use exfoliated layers of beidellite clay which is a member of smectite [23, 24] and achieve a structure in which anatase nanocrystals attach to exfoliate clay layers (ANECL) through the reaction between acidic $TiOSO_4$ and exfoliated beidellite clay under hydrothermal conditions. The ANECL structure is distinctly different from the microporous pillared intercalated layered clay structure, being of a mesoporous structure. In this structure there is no steric hindrance for the formation of anatase nanocrystals. Besides, the anatase nanocrystals retain a large surface area because the aggregation and sintering

of the fine anatase particles are significantly reduced by the exfoliated clay layers. The reactant molecules can readily access and react on the anatase surface through the large pores in the relative open ANECL structure. Furthermore, the pore structure and composition of the catalysts as well as the size of anatase nanocrystals can be controlled by manipulating experimental parameters in the synthesis, such as ratio of titanium to clay (Ti/clay), concentration of titanium salt, hydrothermal thermal temperature. This allows us to optimize the catalysts to meet various requirements in practice. Various techniques, such as X-Ray diffraction (XRD), transmission electron microscopy (TEM) equipped with energy dispersive x-ray spectroscopy (EDS), UV-Visible spectroscopy, N_2 adsorption and FTIR and Raman spectroscopy have been employed to monitor the structural change of the catalysts in this study. We aim for a better understanding of the relationship between the structure and performance of the catalysts and thus to design recyclable photocatalyst with superior activity.

Results and Discussion

TEM. The TEM images of several samples are illustrated in Figures 1-3. In Figure 1 the morphology of the TiO_2-pillared clay (image a), Ti-iso-M, is compared with those of the samples prepared by the new approach, Ti-M5-100, Ti-M10-100 and Ti-M20-100 (images b-d). Generally, the clay layers in all four samples were retained during the preparation. An obvious feature of the samples prepared by the hydrothermal approach is that there are many dark spots with sizes up to 10 nm, which are anatase nanocrystals on the clay layers according to the mass contrast as discussed later. In contrast, there are a few anatase nanocrystals (dark spots) observed in the pillared clay sample (image a). The region marked in Figure 1a is magnified further in Figure 2.

The stacking of clay layers, with the interlayer distance varying from 1.65 to 4.2 nm, can be seen clearly. The interlayer distance for the parent clay is about 0.3 nm, and the increase in interlayer distance is due to the intercalation of clay layers with TiO_2 pillars, as reported in literature.[17, 18] TiO_2 pillared clays usually have wide pore size distributions [25] because of the difficulty in obtaining uniform size of titanium hydrate sol particles, the precursor of pillars.

(Figure 2)

The images of the samples prepared at a high hydrothermal temperature of 200ºC are given in Figure 3. The Ti/clay ratio in the synthesis of these four samples increases from 5 mmol of titanium per gram of clay (mmol/g) for Ti-M5-200 to 20 mmol/g for Ti-M20-200, and there is a trend that the amount of anatase crystals on the clay layers increases with the Ti/clay ratio. At the same time, the rise of the Ti/clay ratio also results in growth of anatase crystal in size. Besides, by comparing the images in this figure with those of the corresponding samples prepared with the same Ti/clay ratio in Figure 1 (for instance, comparing the image of Ti-M5-200 with that of Ti-M5-100), we can realize the influence of the hydrothermal temperature in the new synthesis approach on the structures of the product catalysts. Obviously, the clay layer was seriously damaged (Figure 3) during the synthesis with the hydrothermal treatment at 200ºC. It is also noted that the size of anatase crystals in the high temperature products are obviously larger than those in the corresponding samples prepared at 100ºC.

Another trend is that the higher the Ti/clay ratio, the more serious the damage to the clay layers are observed in the samples prepared at a hydrothermal temperature of 200ºC. In the image of

Ti-M20-200, we mainly see the anatase crystals and there are no recognizable clay layers. The damage of the clay layers is due to acid leaching of the clay.[26-28] The chemical composition of the nanocomposite photocatalysts was determined by x-ray fluorescence (XRF) technique, and the results are listed in Table 1. As anticipated, the compositions of the samples vary with the synthesis conditions, and the compositional changes are accompanied by structural changes. For instance, alumina content decreases with increasing Ti/clay ratio. The aluminum in beidellite clay comes from the sheet of AlO_6 octahedra, which are sandwiched by two sheets of SiO_4 tetrahedra.[29] Thus, the loss of alumina also implies destruction of the clay layers. As the Ti/clay ratio increases, more acidic $TiOSO_4$ was added into the synthesis system, and the acidity of the reaction mixture was stronger, inevitably resulting in more serious acid-leaching reaction.

The result that the high alumina content in the pillared clay sample, Ti-iso-M, suggests that the clay layers in this sample remains almost intact, and this is consistent with the TEM observation that the section area of the layers can be seen clearly (Figure 1). The relation between the sample composition and the Ti/clay ratio is depicted in Figure 4a, and the relation between the composition and the hydrothermal temperature is reported in Figure 4b. For the samples prepared at the same hydrothermal temperature, the content of titania increases with the increasing Ti/clay ratio as anticipated, and this is companied with decrease in the contents of Mg, Al, Si and Fe, especially in aluminium content. The compositional changes convincingly indicate the reaction between clay layers and $TiOSO_4$, with acid leaching of the clay layers during the hydrothermal synthesis.[26-28]

XRD. XRD patterns of the samples are shown in Figure 5. Anatase is the only the crystal phase of titania observed in the XRD patterns of all samples (Figure 5, a-c). The diffraction peaks from

anatase are indexed in the figure according to the PDF card 004-0477. The mean crystal size of anatase was estimated from the full width of half maximum (FWHM) of the (101) peak by the Sherrer equation.

Moreover, the intensity of the diffractions of the beidellite clay provides useful information on the changes in the clay structure. The XRD pattern of beidellite is shown in Figure 5e, and the three strongest diffraction peaks are from (001), (100) and (004) planes according to the PDF card 043-0688. The intensity of these three peaks gradually decreases when the Ti/glay ratio in the synthesis increases (Figure 5 a-c). The peaks from beidellite in the pattern of Ti-M20-200 almost disappear, indicating that the clay layers were destroyed by the acid leaching. The peaks from the clay become weaker when we raised the hydrothermal temperature. It is reasonable that the acid leaching of clay layers is more serious at higher temperatures. In contrast, the diffractions from the beidellite are relative strong in the pattern of the TiO_2-pillared clay sample, Ti-iso-M, and weak diffractions at 25.3º and 48.1º are observed, which could be assigned to the diffractions of the (101) and (200) planes of anatase,. This result suggests that the clay layers in the pillared clay remain almost intact, being in agreement with the TEM result (Figure 1 and Figure 2). This sample contains over 10% titania, and should have given strong diffractions if the titania existed as anatase crystallites. The weak diffractions from anatase imply that the quantity of the anatase in this sample is low. The crystal size of the anatase estimated by Sherrer's equation using the (200) diffraction is 5.7 nm. These anatase crystals should locate on the external surface of the stackings of layered clays while most of the titania pillars in the interlayer space are too small to be crystals. The diffraction peak of the highest intensity in Ti-iso-M appears at 8.98 º, and this 2θ is higher than that of the (001) peak of beidellite. Generally, the intercalation of layered clays with pillars

results in a shift of the (001) peak to a lower 2θ. The peak observed is probably the secondary reflection (002) peak, and the (001) peak could not be detected in this experiment.[30] The d_{001} value is estimated from the secondary peak to be 1.94 nm, which was in harmony with the TEM observation of this sample.

To further understand the formation of the composite structure, specimens were taken from different stages in the synthesis of Ti-M20-200: one was taken before the hydrothermal treatment, labeled as Ti-M20-200(uh) and one taken after the hydrothermal treatment but before washing and calcination, labeled as Ti-M20-200(uc). The XRD patterns of these two samples are illustrated in Figure 5e.

The pattern of the sample before the hydrothermal treatment, Ti-M20-200(uh), is similar to that of the beidellite clay, with lower diffraction intensities from the clay. This means that the clay layers in this sample are well preserved, so that the acid-leaching of the clay is negligible before the hydrothermal treatment. The weaker peak intensities are attributed to the fact that the clay content in this sample is below 50% (Figure 4). The fact that no diffractions of titania could be detected from the pattern suggests that anatase crystals have not formed before the hydrothermal treatment.

In the pattern of Ti-M20-200(uc), the (001) diffraction of the clay becomes a shoulder, and the diffraction intensity from the (004) planes is very weak. It means that the clay layers in this sample were seriously damaged during the hydrothermal treatment which greatly promoted the acid leaching of the clay layers and the formation of anatase crystals. The diffractions from anatase, with high intensities, are observed on this pattern. In the subsequent washing and calcinations, the crystallinity of anatase improved but the clay layers in this sample were totally

destroyed as shown by the pattern of Ti-M20-200 in Figure 5c, in which the diffractions from the clay almost disappear although the silica and alumina still account for about 40% of the mass of this sample (Figure 4). Thus, the process of washing could intensify the collapse of the clay structure. In addition, anatase phase formed during the hydrothermal process. It might result from the acidic environment and appropriate hydrothermal temperature which were beneficial to the formation of crystallites of anatase.

Furthermore, diffraction peaks of a new phase, natroalunite, are also observed in the pattern of sample Ti-M20-200(uc). It appears that the aluminum leached out from the clay layers and interlayer sodium cations formed natroalunite.

UV-Visible: UV-Visible spectra can provide useful information on the band structure of the semiconducting solids of titania as well as on the coordination of titanium in titania solids. Figure 6a-d shows the UV-Visible spectra of the samples. Two peaks around 330 nm and 240 nm are observed. The peak around 330 nm is assigned to the absorption band of anatase, which is also in accordance with charge transfer transition often observed at 333 nm for the octahedral coordination of Ti.[31] The peak around 240 nm should be the absorption band of clay, which is associated with the charge transfer of some other elements in samples. Apparently, the absorption bands of the samples prepared with the same Ti/clay ratio are similar. This means that ratio of Ti/clay influences quite remarkably the size of anatase and the coordination of Ti in the samples. It is also found that as the Ti/clay ratio increases from 5 mmol/g, to 10, 15 and 20 mmol/g, the absorption peak shifts from 316 to 326, 330 and 335 nm, respectively (Figures 6a-6d). There are two possible reasons for the trend of the peak shift. The crystal size of anatase decreases with the

decreasing Ti/clay ratio (Figure 5f), resulting in a wider band gap of anatase. This is the so called quantum size effect and has been observed in a number of semiconducting crystals when the crystal size is below 10 nm.[32-36] Besides, the incomplete coordination of Ti with O, (or the coordination of Ti is of a lower symmetry than octahedral) become more serious in the smaller anatase crystals. The shift of the absorption peak to shorter wavelength (except for samples prepared with a Ti/clay ratio of 20), in relation to adsorption at 333 nm for the octahedral coordination of Ti, is also due to the lower symmetry coordination structure of titanium and oxygen. This peak for Ti-iso-M appears at 316 nm, indicating a small size of anatase and a large number of titanium in this sample exist with incomplete coordination. The increase of the band-gap energy may result from the quantum size effect and the matrix/support effect.[31]

Figure 6f is the UV-Visible spectrum of a 0.5g/L beidellite suspension. It is observed that the beidellite suspension starts to absorb light at 700 nm and has strong absorption between 300 nm and 400 nm. This absorption reduces the irradiation the catalytic active anatase and thus affects the activity of the samples containing beidellite.

N_2 sorption: N_2 sorption is a widely used technique for comprehensive characterization of pore structures of porous solids.[37, 38] N_2 adsorption/desorption isotherms of the samples, and beidellite clay are illustrated in Figure 7. The shape of the isotherm of Ti-iso-M is distinctly different from that of beidellite (Figure 7d) because of the pillaring, which results in large amounts of micropores and mesopores in the pillared clay.[17, 22] The BET specific surface area of beidellite was derived from the nitrogen adsorption data to be 13 m^2/g while the surface area of Ti-iso-M is 190 m^2/g.

The sorption by the ANECL samples is obviously high compared with that of the pillared

clay, Ti-iso-M (Figure 7), proving that these samples have a much larger porosity than the pillared clay.[37] The BET specific surface area and pore volume of the samples were calculated from their adsorption data and are summarized in Table 1. The ratio of the pore volume to the specific surface area is of a dimension of mean pore size,[39] and can be used for comparing the pore sizes of the pillared clay and the ANECL samples approximately. The ratio for ANECL samples is 65% to 260% larger than that of the pillared clay, suggesting that mean pore size in the ANECL samples are much larger than that in conventional pillared clays. It is also noted that the height of the hysteresis loops on the isotherms of the ANECL samples ranges from 80 (Ti-M5-100) to 170 cm^3STP/g (Ti-M20-150) and is much higher than the 30 cm^3STP/g for the pillared clay. The hysteresis is due to the capillary condensation of mesopores (with pore sizes between 2 and 50 nm) in the solids, so that the higher the hysteresis loop, the larger the mesopore volume is. The observation implies that there is a large quantity of mesopores in the ANECL samples, and consequently, there won't be a steric hindrance in the formation of anatase nanocrystals, and organic molecules can diffuse to the anatase crystals without any serious resistance. The fact that most of the hysteresis loops close at a relative pressure p/p_0 between 0.8 and 0.9 units, suggests that most of the mesopores are below 10 nm in size. These structural features are in harmony with the results of TEM and XRD measurements, which indicate large amounts of anatase nanocrystals formed in these samples.

There is a trend that adsorption capacity increases with the increasing Ti/clay ratio. It means that more pores form at a higher Ti/clay ratio. The hysteresis of the pillared clay sample is a H4 type loop characteristic, which is associated with slit-shaped mesopores.[38] This is typical for pillared clays.[23] The mesopores are the void between the stackings of the clay layers. While the

hysteresis loops on the isotherms of many ANECL samples appears a hybrid of H2 and H3 type hysteresis. H2 loops are associated with interconnected network of pores with different size and shape, and often observed for metal oxides; H3 loops are associated with aggregates of platy particles. The H2 component should come from the voids between the anatase nanocrystals, and the H3 component from the pores with pore walls of the damaged clay layers. The conclusion deduced from the isotherms in Figure 7 is consistent with the TEM observation: the pore structure of the ANECL samples is very different from the pillared clay and we can control the pore structure by manipulating the synthesis conditions.

The data of the BET specific surface area and pore volume in Table 1 provide useful information on the sample texture. Among the samples prepared at the same hydrothermal temperature, the sample prepared with the Ti/clay ratio of 10 mmol/g (Ti-M10-x) usually has the largest specific surface area. When the Ti/clay ratio is kept unchanged, raising the hydrothermal temperature usually results in the loss of the specific surface area. The anatase crystals are larger when the samples were prepared with high hydrothermal temperature and the clay layers are more seriously damaged. Both lead to reduction of specific surface area. It is noted that Ti-M15-100E has the largest pore volume (Table 1 and Figure 7a). This sample was prepared with a Ti/clay ratio of 15 mmol/g clay and at hydrothermal temperature of 100°C. The wet cake of the sample was further washed with ethanol (by dispersing the cake in ethanol and recovering the solid by centrifugation) after routine washing with water. The purpose of the “ethanol washing” is to replace water in the wet cake with ethanol which has much lower surface tension compared to that of water. When the ethanol is removed during the subsequent drying procedure, the clay layers are in a form of “cards in house”, which is a more disordered configuration and resembles the

structure of exfoliated clay layers, because of the low surface tension of ethanol. Thus, larger pore volume is retained in the sample. Its specific surface area and pore volume are 75 m^2/g and 0.09 cm^3/g, respectively, larger than those of Ti-M15-100, prepared with the same procedures but without the ethanol washing and before drying and calcinations.

The pore structure of the ANECL solids and pillared clays can affect the formation of anatase crystals and diffusion of the organic contaminant molecules toward the anatase surface, and thus are crucial to the photocatalytic performance. The pore size distribution (PSD) of the samples, over both micropores and mesopores can be derived from the nitrogen sorption data with a method based on the *t*-plot.[39] The accumulation of the surface areas and volumes from all pores in the samples, calculated by this method, are in good agreement with the BET specific surface area and overall pore volume. For most samples, the differences between the BET specific surface area and the accumulated surface area, and between the overall pore volume and the accumulating pore volume, are less than 10%. The PSDs of three samples are illustrated in Figure 8. The titania pillared clay, Ti-iso-M, is mainly a microporous solid with a large amount of micropores (< 2 nm). The Ti-M15-100 is a mesoporous solid and most of the pores in this solid are in a pore size range between 2 and 10 nm. This proves that the washing with ethanol increases the volume of the pores larger than 3 nm substantially.

Raman Spectra. Figure 9a shows the Raman spectra of some ANECL samples. All these peaks in Figure 9a were attributed to the vibration of anatase phase of TiO_2. The spectra around 142 cm^{-1}, E_g adsorption band of large anatase crystallites, are enlarged in Figure 9b. This band blue shifts, and broadens for all samples, in relation to the band of large anatase crystallites. The blue shift and the asymmetrically broadening of the peaks at 142 cm^{-1} and 630 cm^{-1} are associated with

reduction in the anatase crystal size.[40, 41] We can thus put the crystal size of the samples in an order according the blue shift as below:

Ti-M20-200 > Ti-M20-100 > Ti-M15-100 > Ti-M10-100 > Ti-M5-100 > Ti-iso-M.

This sequence is identical with that obtained from the XRD results. Actually, the crystal size of the samples calculated from Raman spectra using the method reported in literature [40] is about 3 nm smaller than that calculated from the XRD data. For instance, the crystal size of anatase on sample Ti-M20-200 calculated by Raman spectra is about 10 nm, whereas that calculated by XRD is about 13.4 nm. The reason of this phenomenon is not clear and might result from the interaction of the anatase crystal with the clay structure. The Raman spectrum of Ti-iso-M shows that the titania in this sample has poor crystallinity, as anticipated.

The Raman spectra also provide information on the structural changes in the clay layers. The peaks at 700 cm^{-1} in the spectra of Ti-iso-M and Ti-M5-100 samples were ascribed to beidellite, which gradually disappeared as the lay structure was destroyed. This result is in harmony with that of XRD.

FTIR. Figure 10 shows the FTIR spectra of the samples, which provide information on the structural evolution during the catalyst synthesis. Figure 10a and 10b are the IR spectra of beidellite in the range of 800 to 1250 cm^{-1} and 2900 to 3800 cm^{-1}, respectively. The bands at about 915, 882 and 849 are assigned to the Al-O-Al-OH, Al-O-Fe-OH and Al-O-Mg-OH vibrations of beidellite, respectively.[42-46] The band at 948 cm^{-1} is for the Al-OH in plane vibration mode.[42] The band around 1080.8 cm^{-1} is assigned to the out-of-plane vibration for Si-O bond and those around 983.4, 1032.7 and 1112.9 cm^{-1} are assigned to the in-plane vibrations of Si-O bond. [42, 47, 48]

The band at 3628.2 cm^{-1} in Figure 10b is attributed to the Al_2OH vibration and that at about 3400 cm^{-1} is the vibration of the hydroxyl groups involved in water-water hydrogen bonds. The band at bout 3560 cm^{-1} was the vibration of hydrogen bonds to oxygen of Si-O-Si linkages. The band at about 3250 cm^{-1} is ascribed to an overtone of the water bending vibration that lies near 1630 cm^{-1}, but absorption below 3200 cm^{-1} is enhanced by the presence of small, strong polarizing cations, such as Al^{3+}, since water molecules coordinated to them form stronger water hydrogen bonds in outer spheres of coordination.[42]

Comparing the IR spectra of sample Ti-M20-100 with those of the parent beidellite, one can find that the Si-O-Si in-plane stretching band around 980 cm^{-1} disappears, leaving the in-plane bands around 1030 cm^{-1} and 1110 cm^{-1} only. This is because the aluminum was leached out during the hydrothermal treatment and beidellite was damaged, forming small silica particles. As a result, the stretching vibration frequency of the Si-O-Si bonds increased. Also, a new band emerged around 1185 cm^{-1} and is assigned to the terminal Si-O_t bonds.[42] The damaged layers have significantly more terminal Si-O_t bonds exposed. Meanwhile it is also observed in Figure 9c, that for Ti-M20-100, the vibrations of Al-O-Al-OH, Al-O-Fe-OH and Al-O-Mg-OH, at 915, 882 and 849 cm^{-1} respectively, became weaker than the corresponding band for beidellite (in Figure 9a). In addition, the peak assigned to the in-plane vibration of Al-OH at 946 cm^{-1} disappears and the sharp peak of the vibration of Al_2OH at 3626 cm^{-1} in Figure 9b became a shoulder in Figure 10d. These observations can be attributed to leaching out of aluminum in the octahedral layer as indicated by the chemical compositions of Ti-M201 and beidellite in Table 1. Furthermore, a new band at 966 cm^{-1} is observed in Figure 10c, and is attributed to the vibration of the bonds of Si-O-Ti.[49] This band suggests that anatase crystals are strongly bonded to the silicate through a

chemical bond, which is also beneficial to the stability of the anatase.[50, 51]

Photocatalytic Activity: The activities of the catalysts for degrading phenol in aqueous solution under UV irradiation are illustrated in Figure 11. The ANECL samples exhibit better activity than that of the titania pillared clay, Ti-iso-M. In general, for the catalysts prepared at the same hydrothermal temperature, the activity of the catalysts improves as the Ti/clay ratio increases; while for the samples prepared with the same Ti/clay ratio, the activity declines with increasing hydrothermal temperature, *i.e.*, the samples prepared at 100°C show the best activity. The strongest activity is observed for Ti-M15-100E. The "ethanol washed" sample is obviously superior to all other samples in catalytic activity (Figure 11). The better activity is attributed to important structural changes induced by ethanol washing.

The products of the photocatylytic reaction were analyzed by high performance liquid chromatography (HPLC) using a XDB-C8 column and reaction intermediates were observed. The analytical results of specimens, taken from the reaction system with Ti-M20-100 as photocatalyst after various reaction periods are shown in Figure 11d. There are four different intermediates (indicated by the arrows), and are analysed as hydroquinone, resorcin, pyrocatechol and benzoquinone according to the literature.[52, 53] The concentration of intermediates is related to the phenol concentration in the solution. The mechanism of the phenol degradation has been extensively discussed.[52, 53] Generally, it is believed that phenol molecules are oxidized by OH• radicals produced by the photocatalysts.[2, 52, 53] The photons of UV light excite electrons in valence band to conduction band, yielding electrons and holes in conduction and valence bands, respectively, and the OH^- groups adsorbed on the surface of the catalyst lose an electron to the

holes and form the OH• radicals. The HPLC results indicate that phenol molecules are first oxidized to intermediates, and eventually to carbon dioxide and water.

Reaction of the synthesis: As the above results show, the ANECL samples formed through a reaction under hydrothermal conditions, are distinctly different from the pillaring intercalation process, so that we can achieve a very different structure that is more efficient for the photocatalytic degradation of organic pollutants such as phenol. We found that titanium hydrate precipitate could form from the titanium source in this synthesis, $TiOSO_4$, when its aqueous solution was hydrothermally treated under the same condition but without the clay. Therefore, it is believed that the titanium hydrate species in an aqueous $TiOSO_4$ solution form large and positively charged oligomers readily during the hydrothermal conditions in an acidic media, which then convert into anatase nanocrystals. At the same time, large quantity of H_2SO_4 is released which reacts with the clay layers, leaching out aluminum and damaging the layer structure. When the clay layers are swelled and exfoliated in advance, the positively charged precursors of anatase nanocrystals, can disperse homogeneously among the clay layers carrying negative charges, and the leaching reaction is enhanced. More importantly, in this approach there is no steric restriction on the size of the anatase crystals so that most of the TiO_2 in the ANECL samples exist in anatase nanocrystals which are active to the photodegradation of organic pollutants. Another distinct feature of this synthesis is that the hydrothermal treatment which was usually avoided in the preparation of pillared clays to prevent the clay layers from the damages caused by acid leaching. In fact, the structure with registration of parallel layers is not important for photocatalysts. While the hydrothermal treatment facilitate the formation of anatase crystals and one can tailor the

crystals size readily by altering the Ti/clay ratio and hydrothermal temperature.

These nanocrystals are linked to damaged clay layers through chemical bonds as evidenced by the FTIR results. This linkage brings about two important benefits. Firstly, the formation of Ti-O-Si bonds might stabilize the anatase nanocrystals, according to literature.[50, 51] This will ensure the stable performance of the ANECL photocatalysts. Secondly, the anatase crystals attached to the large silicate piece, so that they can be readily separated from solution after the reaction, simply by sedimentation or filtration. While most the TiO_2 catalysts of fine powders encounter the difficulties on the separation. This impedes their practical application although they exhibit superior photocatalitic activity.[54]

Relation between catalytic activity and catalyst structure: The superior activity of these catalysts originates from their unique structure. Consider the structural difference illustrated in Figure 8 and the difference in photocatalytic activity of the three samples. It seems that the mesopores larger than 3 nm have important influence on the catalytic activity. The volumes of these mesopores were calculated for all the samples and are plotted against their activity expressed in the percentage of the phenol that were degraded over the catalysts (Figure 12). A general trend observed in the top panel is that the samples with a larger mesopore volume exhibit better activity, although some points disperse away from the dash line which indicates the trend. When the samples are grouped according to the hydrothermal treatment temperature, as shown in the bottom panel, the point is much less dispersed. At the same hydrothermal temperature, the extent of the reaction between the clay layers and $TiOSO_4$ may be similar and so does the crystallinity of the anatase nanocrystals. The trend demonstrated in Figure 12 verifies our hypnosis that the

photocatalytic activity could be improved by forming mesoporous system and anatase nanocrystals as the photocatalyst. In the ANECL samples titania disperses on the fragments of the damaged clay layers, existing small anatase crystals with a size between 3 and 10 nm. Moreover, the crystals are accessible to organic pollutants and oxygen molecules through the mesopores, and simultaneouly to the UV light.

The photocatalytic process is a complicated heterogeneous catalytic system, there are a number of factors influencing the photocatalytic process, such as the pore structure, anatase crystals, the ability of the catalyst to be dispersed in water, etc. For instance, beidellite suspension absorbs the light in 300-400 nm of the wavelength (Figure 6f) and this has an adverse effect on the activity of samples prepared from beidellite because the less photons of UV irradiation are absorbed by anatase nanocrystals for the exiting of the electrons. On the other hand, the Ti-M15-100E is very easily dispersed in water, compared to the titania pillared clay as well as other ANECL samples, this property enhances its activity. All the ANECL samples inherit the properties of pillared clay, which can be separated readily by sedimentation.

Conclusion

The structure of anatase nanocrystals attached to exfoliated clay layers can be formed by a reaction between $TiOSO_4$ and beidellite clay under hydrothermal conditions. The reaction extent and the properties of the anatase crystals in the products depend on the hydrothermal temperature and Ti/clay ratio. The reaction results in a large mesoporosity which facilitates the formation of anatase nanocrystals and diffusion of the organic molecules to the anatase surface where the active sites for the degradation are found. The anatase crystals are linked to the fragments of the acid

leached clay layers through chemical bonds. We find that the catalytic activity increases with the increasing volume of the pore larger than 3 nm because formation of mesoporous system and anatase nanocrystals leads to improvement in the photocatalytic activity of photocatalyst. This new structure is a more efficient photocatalyst structure for degradating organic pollutant in water, compared to the conventional titania pillared layered clay. An ethanol washing procedure can further enhance the mesoporosity and thus the photocatalytic activity. The knowledge acquired in this study is useful for design photocatalysts with high efficiency.

Experimental Section

General: The UV light source was 38 W Hg lamps (NEC, FL15BL T8), and the peak of the wavelength was at about 350 nm. The catalyst concentration was 0.5 g/L, and the initial concentration (C_0) of the phenol was 25 ppm. Prior to irradiation, the dispersion of the catalyst powder and the phenol solution in a Pyrex glass vessel was bubbled with air in the dark for 10 min in order to establish an adsorption/desorption equilibrium of phenol on the catalyst. During the reaction, the liquid of the reaction system was automatically sampled every thirty minutes, and the sample was filtered through a Millipore filter prior to the analysis to remove the catalyst particles. The filtrates were analyzed by a high performance liquid chromatography (HPLC), Agilent, HPLC-Circa 2000, equipped with an Eclipse XDB-C8 column (5μm, 4.6×150mm). The eluent we used were actonitrille (HPLC grade) and 0.1% of acetic acid (HPLC grade). The nitrogen adsorption-desorption isotherms were measured by volumetric method on an automatic adsorption instrument (Micromeritics, Tristar 3000). Prior to measurement, the samples were outgassed at 120 °C for at least 16 h. The nitrogen adsorption-desorption data were recorded at liquid nitrogen temperature (77 K). Specific surface area was calculated by the Brunauer- Emmett-Teller (BET) method from the data in a P/P_0 range between 0.05 and 0.2. The *t*-plot method was applied to calculate the micropore volume and external surface area (mesopore surface area). X-ray diffraction (XRD) patterns of the sample powders were recorded using Cu Kα radiation (λ= 0.15418 nm) on a Philips PANalytical X'Pert PRO diffractometer operating at 40 kV and 40 mA with a fixed slit. The scan rate was 0.725 °(2θ)/min. The infrared spectra of the samples were recorded on a NEXUS 870 Fourier transform spectrometer (Thermo Nicolet Corp.) the mercury cadmium telluride detector were used to record the attenuated total reflection (ATR) spectrum of the sample. Each spectrum was obtained by averaging 64 interferograms with resolution of 4 cm^{-1}. The TEM images of the samples were obtained with A Philips CM 200 transmission electron microscope operating at 200 kV. All samples were ground and scattered on the carbon-coated film directly without any other disposal. The major chemical composition of the samples was determined by XRF technique on a PHILIPS PW2400 XRF instrument. The UV-Visible spectra of

the samples were recorded on a Cary 100 spectrometer and the scan band was from 200 nm to 900nm. Raman spectra were collected by a Spectra-Physics model 127 He-Ne laser (633 nm) at a resolution of 2 cm^{-1} in the range between 100 and 1600 cm^{-1}. Repeated acquisitions using the highest magnification were accumulated to improve the signal-to-noise ratio in the spectra. Spectra were calibrated using the 520.5 cm^{-1} line of a silicon wafer.

Materials. The beidellite, from Southern Clay Products Inc. and with a commercial name of Cloisite Na^+, were used as starting materials to prepare the nanocomposite samples. The clays were used as received. The titanium(Ⅳ) isopropoxide, from Aldrich, was used as received without any purification to prepare the sol of titanium hydrate. The $TiOSO_4$ •xH_2O (98%) and hydrochloride acid (36%) were from Fluka and used as received.

Preparation. 4.0 g of clay was dispersed into 200 ml of deionized water, and the suspension was stirred until it became homogeneous. Stock $TiOSO_4$·solution was prepared by dissolving 128.0 g of $TiOSO_4$·xH_2O into 1.0 L of deionized water and stirring the solution until it became clear (about 40 min). To the clay suspension a designated amount of the $TiOSO_4$ solution was added drop-wise, under vigorously stirring. The mixture was stirred for 3 h before it was transferred into an autoclave and kept at a designated hydrothermal temperature for 24 h. The hydrothermal treatment was conducted at 100, 150 and 200 °C, respectively, to examine the influence of the hydrothermal temperature on the structure, and thus the performance of the photocatalysts. The samples were also prepared with different ratios of titanium to clay (Ti/clay) to investigate the effect of this ratio by using different quantities (25, 50, 75 and 100 ml) of the stock $TiOSO_4$·solution and the same amount of clay suspension in the synthesis. The solid in the autoclaved mixture was separated by centrifugation, and washed with deionized water several times to remove the soluble components. The obtained wet cake was dried in air and calcined at 500˚C for 20 h. The temperature was raised at a rate of 2 °C/min. The last digit in the sample name presents the hydrothermal temperature: numbers 100, 150 and 200 denote hydrothermal temperatures 100ºC, 150ºC and 200ºC, respectively. The number after the letters "Ti-M" indicates the Ti/clay ratio in mmol of [Ti] per gram of clay (mmol/g) in the synthesis, which are 5, 10, 15 and 20 respectively. For instance, Ti-M10-150 is the sample prepared with a Ti/clay ratio of 10 mmol/g and the hydrothermal temperature was150 ºC.

For comparison beidellite pillared with titania particles was prepared by a conventional pillaring intercalation procedure.[17, 18] The pillaring solution was prepared by hydrolyzing titanium(Ⅳ) isopropoxide. 6.45 g of titanium(Ⅳ) isopropoxide, $Ti[OCH(CH_3)_2]_4$ was added into 88 mL of 1 M HCl solution dropwise while stirring vigorously, the molar ratio of [Ti]/[H] was 1:4. The resulting slurry was stirred until it became clear (2-3 h). A total of 2.0 g of clay was dispersed into 200 mL of deionized water. The obtained suspension was stirred for 2 h to make it homogeneous and left overnight. The obtained titanium sol was added to the clay suspension, and the mixture was stirred for another 2 h. The Ti/clay ratio of the mixture was 11 mmol/g. Next, the solid was recovered by filtration and washed it with deionized water for 5 times. The washed cake was dried in the air, and then calcined at 500 °C for 20 h. The calcination temperature was raised at a rate of 2 °C/min. The samples were labeled Ti-iso-M.

Acknowledgement:

The authors are grateful to the Australian Research Council (ARC) and NSFC (90206043) of China.

[1] A. Fujishima, K. Hashimoto, T. Watanabe, *TiO_2 Photocatalysis Fundamentals and Applications*. BKC, Inc., Tokyo, **1999**
[2] A. L. Linsebigler, G. Lu, J. T. Jr. Yates, *Chem. Rev*. **1995**, *95*, 735-758.
[3] M. Anpo, *Pure Appl. Chem.* **2000**, *72*, 1265-1270.
[4] D. Beydoun , R. Amal, G. K-C. Low, S. McEvoy, *J. Phys. Chem. B*, **2000**, *104*, 4387-4396.
[5] H. Y. Zhu, J. Orthman, J-Y. Li, J-C Zhao, G. J. Churchman, E. F. Vansant, *Chem. Mater.* **2002**, *14*, 5037-5044.
[6] J. F. Tanguay, S. L. Suib, R. W. Coughlin, *J. Catal*. **1989**, *117*, 335-347.
[7] C. Ooka, H. Yoshida, M. Horio, K. Suzuki, T. Hattori, *Appl. Catal. B: Environ*. **2003**, *41*, 313-321.
[8] H. Murayama,; K. Shimizu,; N. Tsukada,; A. Shimada,; T. Kodama,; Y. Kitayama, *Chem. Commun.* **2002**, 2678-2679.
[9] R. T. Yang, W. Li, *J. Catal.* **1995**, *155*, 414-417.
[10] R. Q. Long, R. T. Yang, *J. Catal.* **2000**, *196*, 73-85.
[11] L. Chmielarz, P. Kustrowski, M. Zbroja, A. Rafalska-Lasocha, B. Dudek, R. Dziembaj, *Appl. Catal., B: Environ.* **2003**, *45*, 103-116.
[12] H. J. Chae, I. S. Nam, S. W. Ham, S. B. Hong, *Appl. Catal., B: Environ*. **2004**, *53*, 117-126.
[13] S. A. Bagshaw, R. P. Cooney, *Chem. Mater*. **1993**, *5*, 1101-1109.
[14] J. Jamis, A. Drljaca, L. Spiccia, T. D. Smith, *Chem. Mater*. **1995**, *7*, 2086-2089.
[15] J. L. Valverde, P. Sanchez, F. Dorado, C. B. Molina, A. Romero, *Microp. Mesop. Mater.* **2002**, *54*, 155-165.
[16] P. B. Malla, S. Komarneni, *Clays & Clay Miner.*, **1990,** *38*, 363-372.
[17] J. Sterte, *Clays & Clay Miner.*, **1986,** *34*, 658-664.
[18] S. Yamanaka, T. Nishihara, M. Hattori, Y. Suzuki, *Mater. Chem. Phys*. **1987**, *17*, 87-101.
[19] R. Burch, *Ed. Pillared Clays, Catalysis Today*, Elsevier: New York, **1988**, Vols. 2 and 3.
[20] T. J. Pinnavaia, *Science* **1983**, *220*, 365-371.
[21] Z. Ding, H. Y. Zhu, G. Q. Lu, P. F. Greenfield, *J. Colloid Interface Sci***. 1999,** *209*, 193-199.
[22] H. Yoneyama, S. Haga, S. Yamanaka, *J. Phys. Chem*. **1989**, *93*, 4833-4837.
[23] J. T. Kloprogge, J. B. Jansen, J. W. Geus, *Clays & Clay Miner.* **1990**, *38*, 409.
[24] J. T. Kloprogge, *Appl. Clay Sci*. **2006**, *31*, 165-179.
[25] H. Y. Zhu, N. Maes, A. Molinard, E. F. Vansant, *Micro. Mater.* **1994**, *3*, 235-243.
[26] A. Corma, A. Mifsud, E. Sanz, *Clay Miner*. **1987**, *22*, 225-232.

[27] R. Mokaya, W. Jones, *J. Catal*. **1995**, *153,* 76-85.
[28] H. Kaviratna, T. J. Pinnavaia, *Clays Clay Miner*. **1994,** *42,* 717-723.
[29] A. C. D. Newman, *Chem. Clays and Clay Miner.* Longmans, London, **1987**.
[30] M. L. Occelli, P. A. Peaden, G. P. Ritz, P. S. Iyer, M. Yokoyama, *Microporous Mater.*, **1993**, *1*, 99-113.
[31] X. Gao, E. W. Israel, *Catal. Today.* **1999**, *51*, 233-254.
[32] M. Steigerwald, L. E. Acc. Brus, *Chem. Res.* **1990**, *23*, 183-188.
[33] Y. Wang, N. J. Herron, *Phys. Chem.* **1991**, *95*, 525-532.
[34] P. V. Kamat, B. Patrick, *J. Phys. Chem.* **1992**, *96*, 6829-6834.
[35] A. P. Alivisatos, *J. Phys. Chem.* **1996**, *100*, 13226-13239.
[36] B. O. Dabbousi, J. Rodiguez-Viejo, F. V.Muikulec, J. R. Heine, H. Mattoussi, R. Ober, K. F. Jensen, M. G. Bawendi, *J. Phys. Chem.* **1997**, *101*, 9463-9475.
[37] S. J. Gregg, K. S. W. Sing, *Adsorption, Surface Area and Porosity*, 2nd ed. Academic Press: New York, **1982**
[38] F. Rouquerol, J. Rouquerol, K. Sing, *Adsorption by Powders and porous solids, principles, methodology and applications*. Academic Press, London, **1999**, 204.
[39] H. Y. Zhu, P. Cool, E. F. Vansant, B. L. Su, X. P. Gao, *Langmuir*. **2004**, *20*, 10115-10122.
[40] K. Sean, H. P. Fred, T. Micha, *J. Phys. Chem. B,* **1997**, *101*, 2730-2734.
[41] W. F. Zhang, Y. L. He, M. S. Zhang, Z. Yin Q. Chen, *J. Phys. D: Appl. Phys.* **2000**, *339*, 912-916.
[42] V. C. Farmer, *The Infrared Spectra of Minerals. Monograph 4, Mineralogical Society*, London, **1974**, 539
[43] B. A. Goodman, J. D. Russell, A. R. Fraser, F. W. D. Woodhams, *Clays and Clay Minerals*, **1976**, *24*, 53-59.
[44] J. D. Russell, A. R. Fraser, *Infrared methods in clay mineralogy.* London, **1994**.
[45] D. Vantelon, M. Pelletier, L. J. Michot, O. Barres, F. Thomas, *Clay Minerals*, **2001**, *36*, 369-379.
[46] L. Sebebastien, L. Bruno, M. Fabrice, B. Andreas, J. Michel, P. Alain, *Clays and Clay Minerals*, **2005**, *53*, 597-612.
[47] V. C. Farmer, J. D. Russell, *Spectrochim. Acta.* **1964**, *20*, 1149-1173.
[48] V. C. Farmer, J. D. Russell, *Spectrochim. Acta* **1966**, *22*, 389-398.
[49] V. M. Gun'ko, V. I. Zarko, V. V. Turov, R. Leboda, et al, *J. Colloid Interface Sci.* **1998**, *198*, 141-156.
[50] C. Anderson, A. J. Bard, *J. Phys. Chem. B*, **1997**, *101*, 2611-2616.
[51] S. R. Kumar, C. Suresh, A. K. Vasudevan, N. R. Suja, P. Mukundan, K. G. K. Warrier, *Mater. Lett.* **1999**, *38*, 161-166.
[52] A. Mylonas, E. Papaconstantinou, *Polyhedron*, **1996**, *15*, 3211-3217.
[53] E. Naffrechoux, S. Chanoux, C. Pettier, J. Suptil, *Ultrasonics Sonochemistry.* **2000**, *7*, 255-259.
[54] H. Y. Zhu, X. P. Gao, Y. Lan, D. Y. Song, Y. X. Xi, J.C. Zhao, *J. Am. Chem. Soc*. **2004**, *126*, 8380-8381.

Table 1 Specific surface area (BET S.A.) and pore volume (V_p)[a] of the samples.

Sample name	BET S.A. (m^2/g)	V_p (cm^3/g)	Sample name	BET S.A. (m^2/g)	V_p (cm^3/g)
Ti-M5-100	185	0.241	Ti-M5-200	123	0.229
Ti-M10-100	215	0.270	Ti-M10-200	132	0.305
Ti-M15-100	183	0.274	Ti-M15-200	138	0.345
Ti-M20-100	205	0.296	Ti-M20-200	99	0.282
Ti-M5-150	120	0.237	Ti-iso-M	190	0.150
Ti-M10-150	200	0.305	Ti-M15-100E	238	0.373
Ti-M15-150	164	0.257	Beidellite	13	0.075
Ti-M20-150	195	0.362	----------	----------	----------

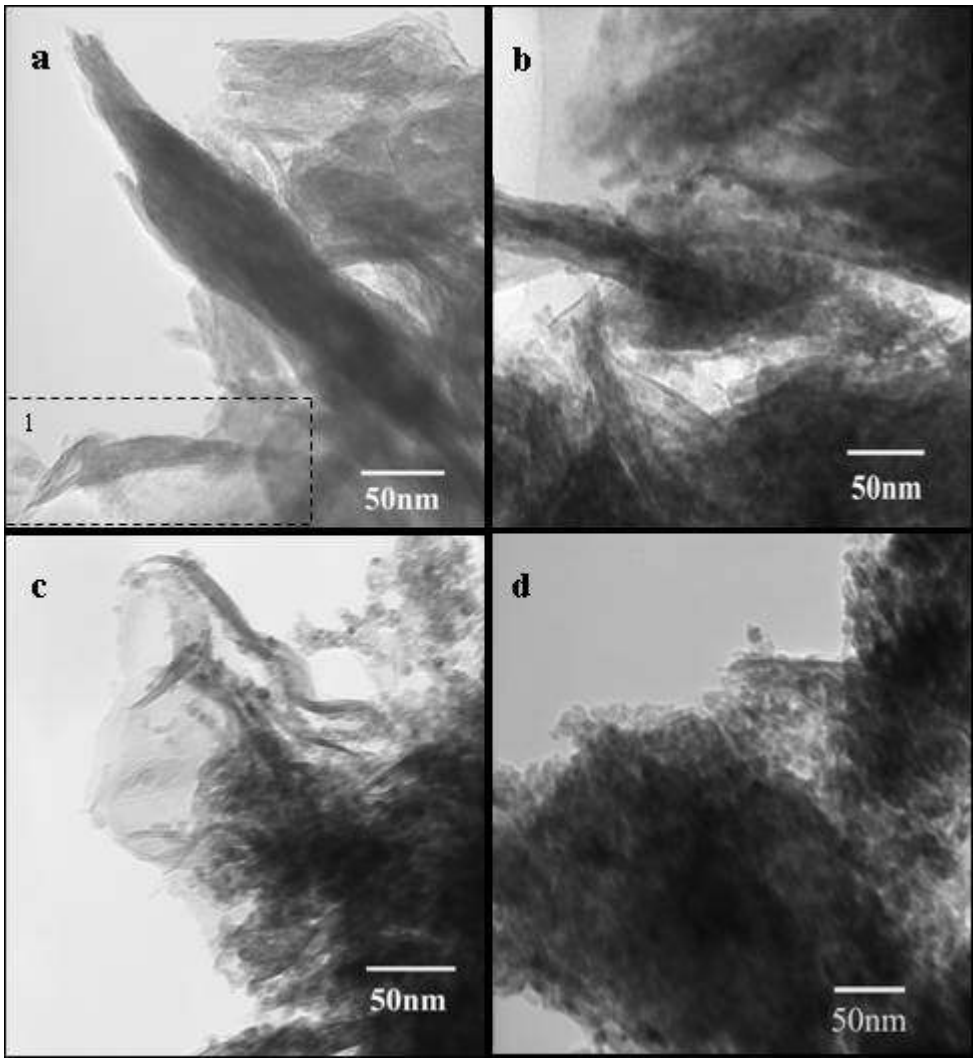

Figure 1. TEM images of sample Ti-iso-M, Ti-M5-100, Ti-M10-100 and Ti-M20-100

Figure 2. High resolution TEM image of the section area of a stacking clay layers (the area highlighted in Figure 1).

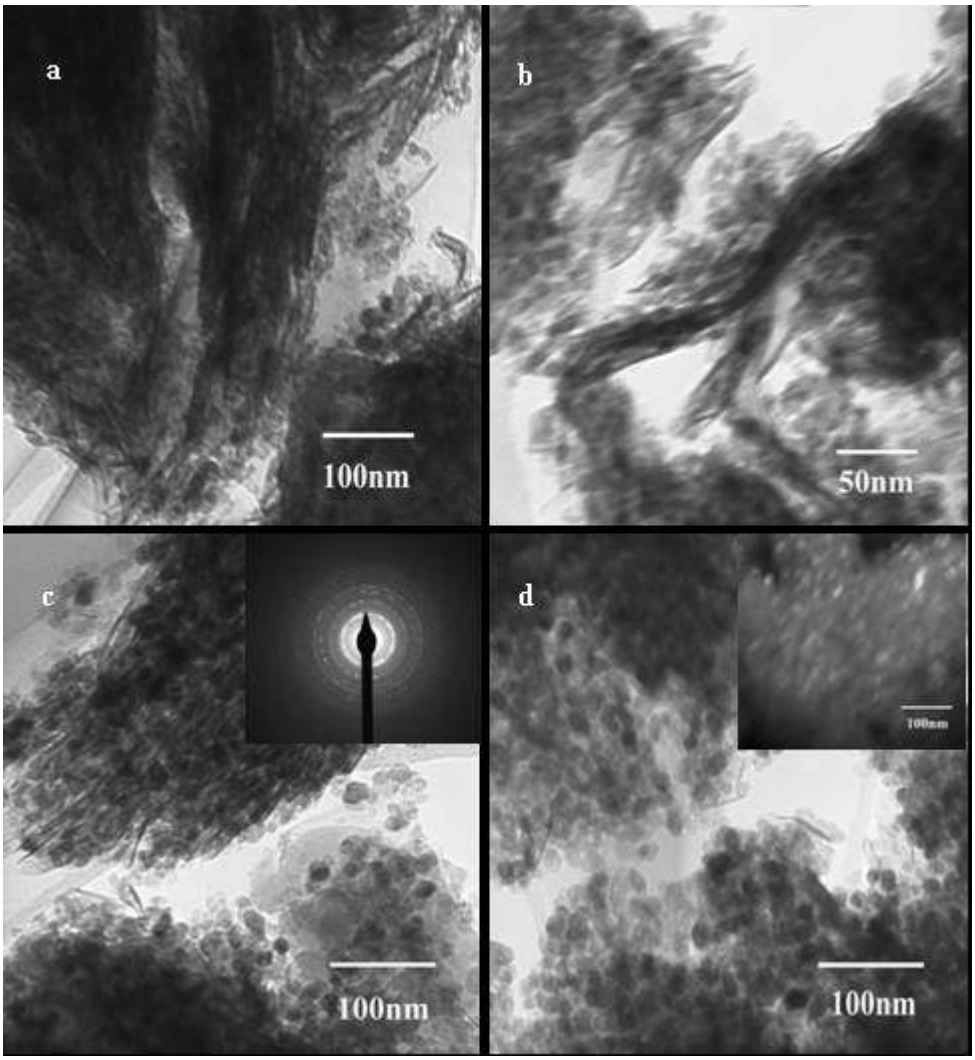

Figure 3. TEM images of Ti-M5-200 (a), Ti-M10-200 (b), Ti-M15-200 (c) and Ti-M20-200 (d) samples prepared at 200ºC.

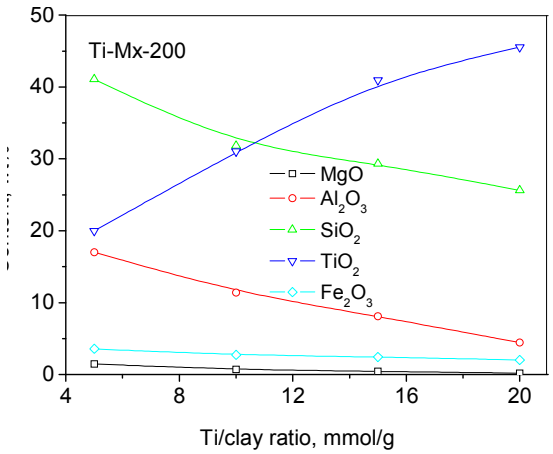

a

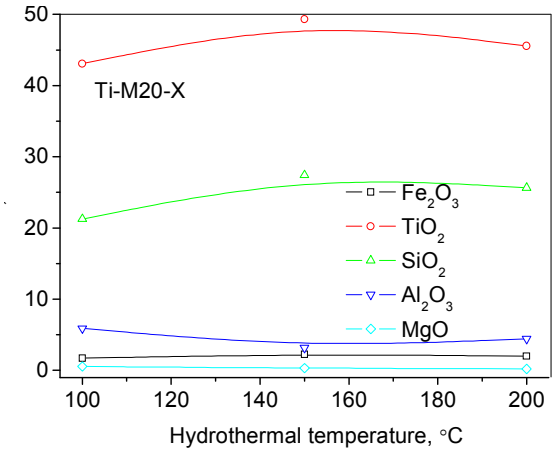

b

Fig. 4. Relation between the sample composition and the ratio of Ti/clay (panel a), and between the sample composition of and the hydrothermal temperature (panel b).

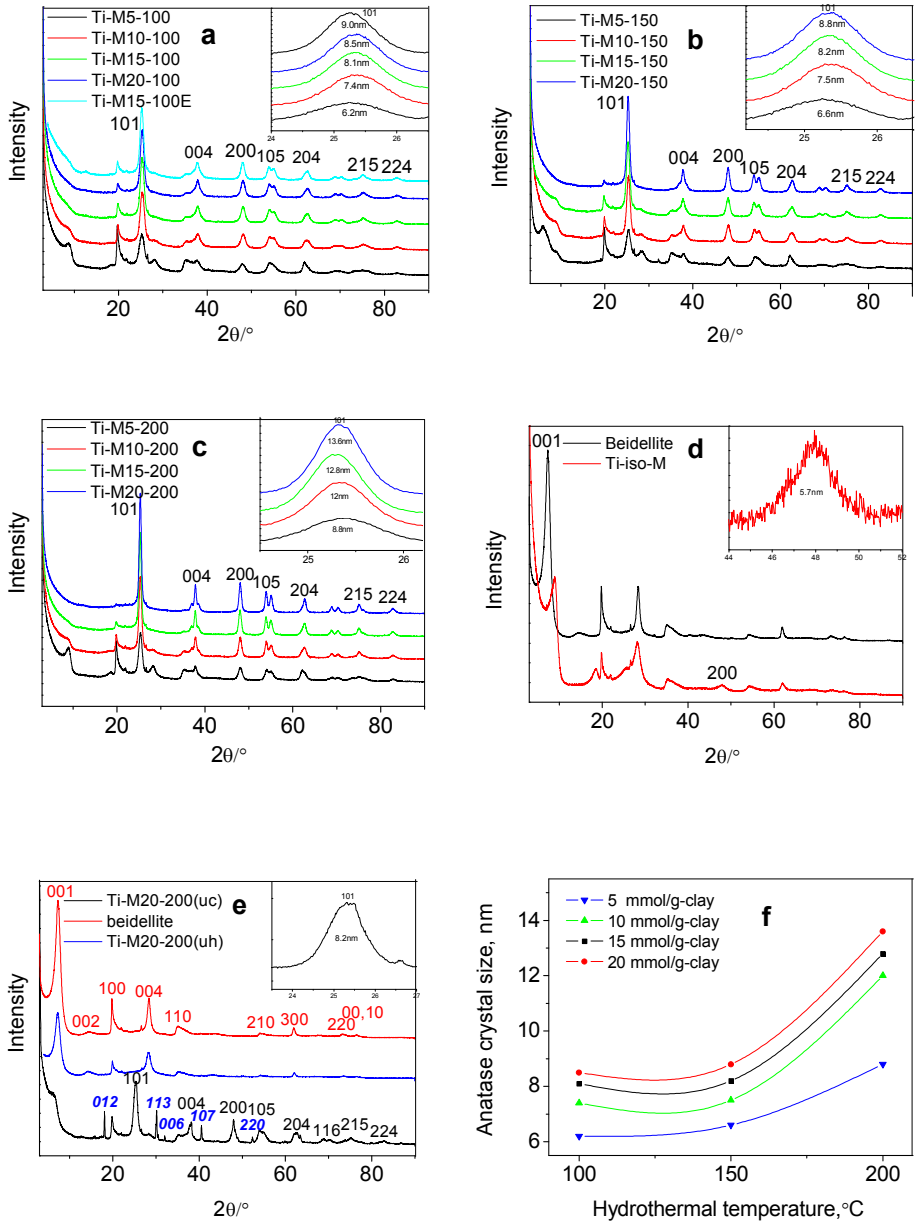

Figure 5. The influence of the synthesis conditions on the structure of the samples. The XRD patterns of the samples prepared at a hydrothermal temperature of 100ºC, 150ºC, and 200ºC are illustrated in panels a, b, and c, respectively. The XRD patterns of Beidellite and Ti-iso-M are in panel d. The patterns of Ti-M20-200 (uh) and Ti-M20-200 (uc) are compared with that of Beidellite in panel e. The relationship between anatase crystal size and the hydrothermal temperature and the Ti/clay ratio is depicted in panel f.

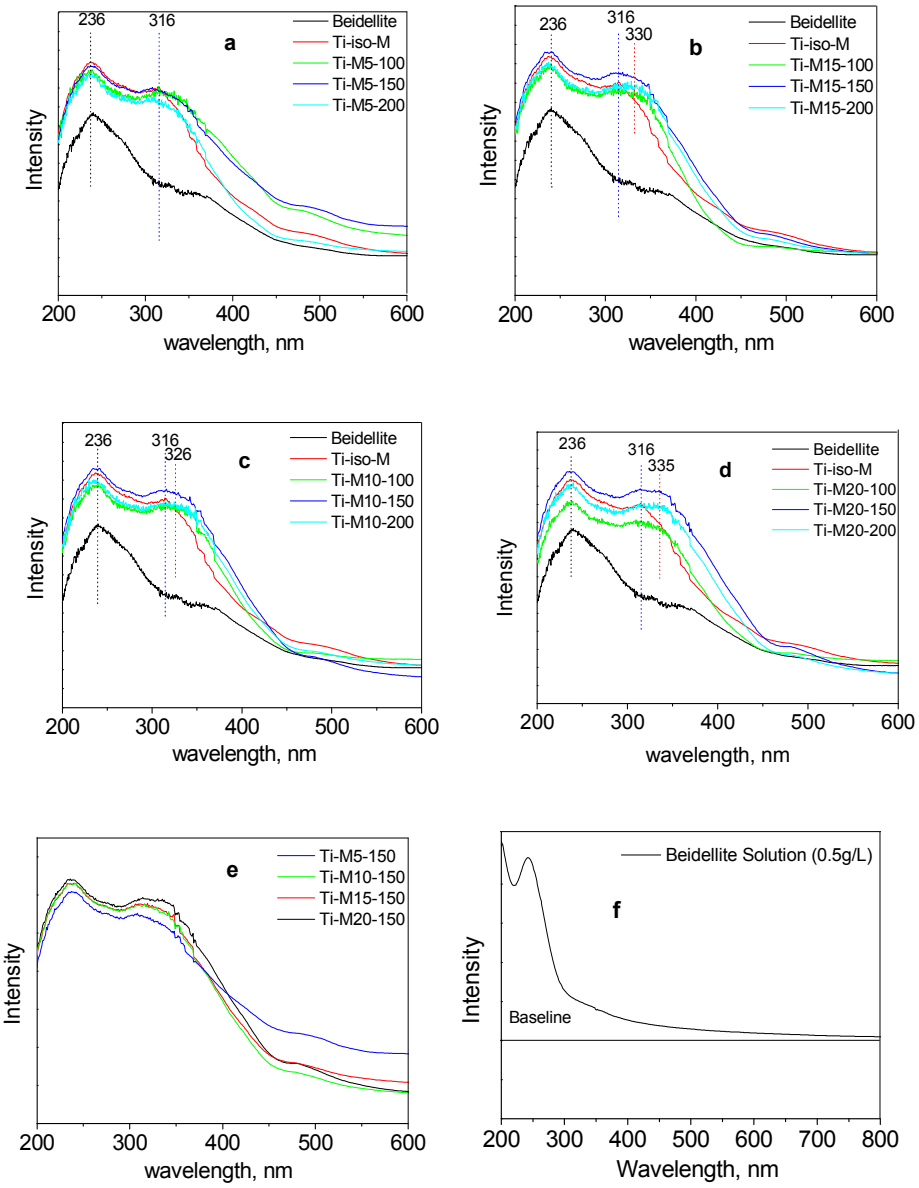

Figure 6. UV-visible spectra of the samples with a Ti/clay ratio of 5 mmol/g (panel a), 10 mmol/g (panel b), 15 mmol/g (panel c) and 20 mmol/g (panel d). The spectrum of the Beidellite suspension is also given in panel e for comparison.

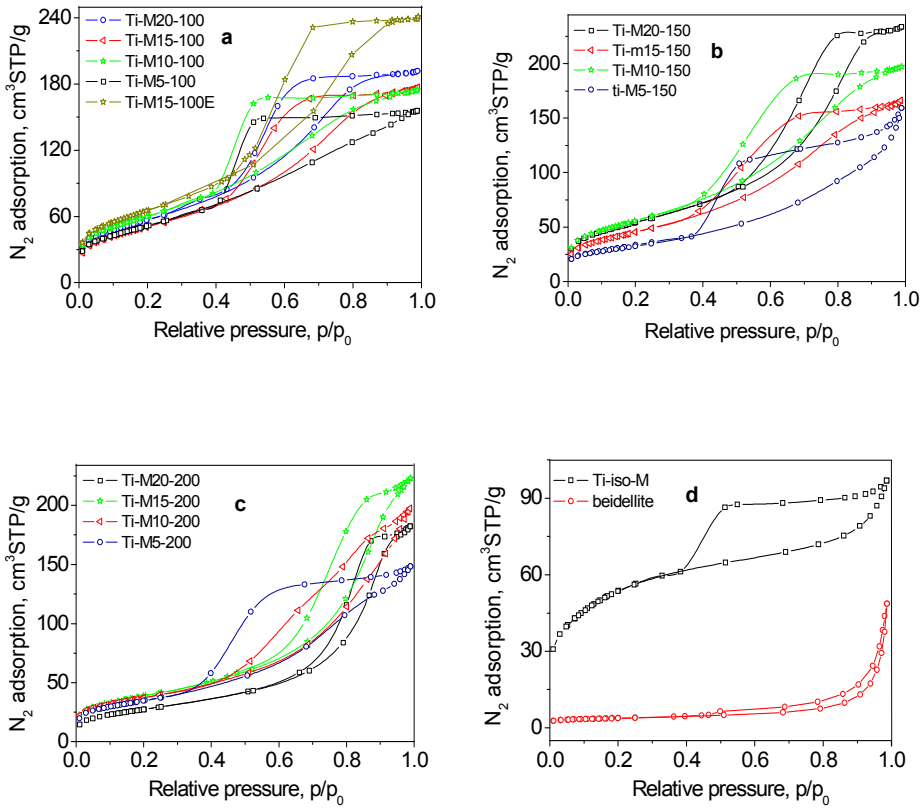

Figure 7 N_2 sorption isotherms of the samples prepared at a hydrothermal temperature at 100ºC (panel a), 150ºC (panel b) and 200ºC (panel c), The isotherms of Ti-iso-M and Beidellite samples are shown in panel d.

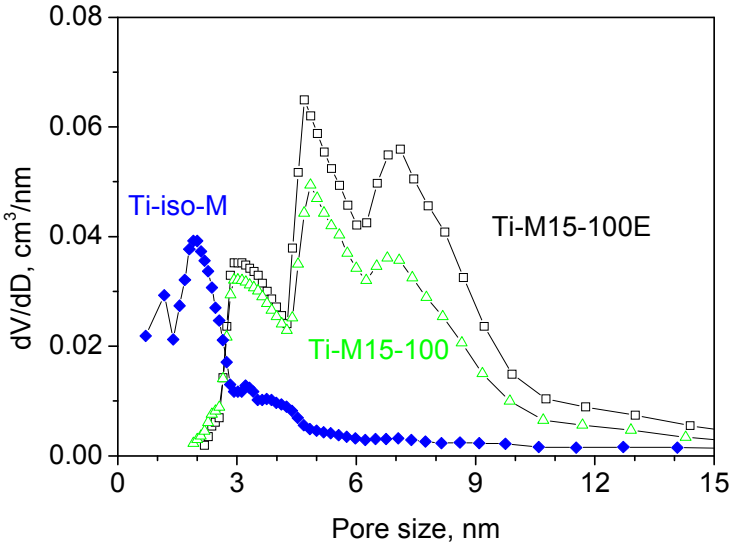

Figure 8. Pore size distribution of the samples Ti-iso-M, Ti-M15-100 and Ti-M15-100E.

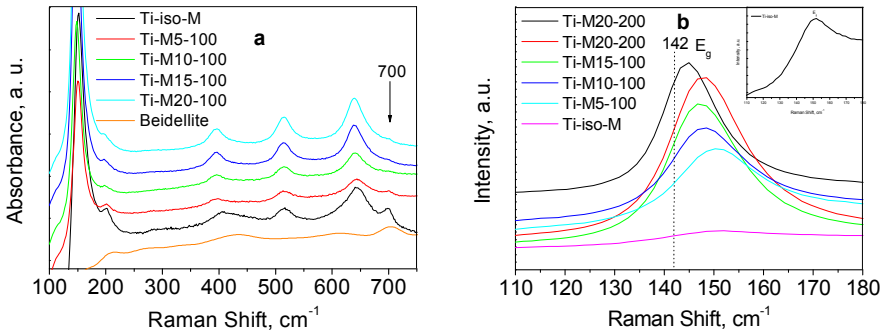

Figure 9. Raman spectra of some samples are shown on the left-hand-side panel and the Raman shift at 142 cm^{-1} for samples are enlarged in the right-hand-side panel to show the shift more clearly.

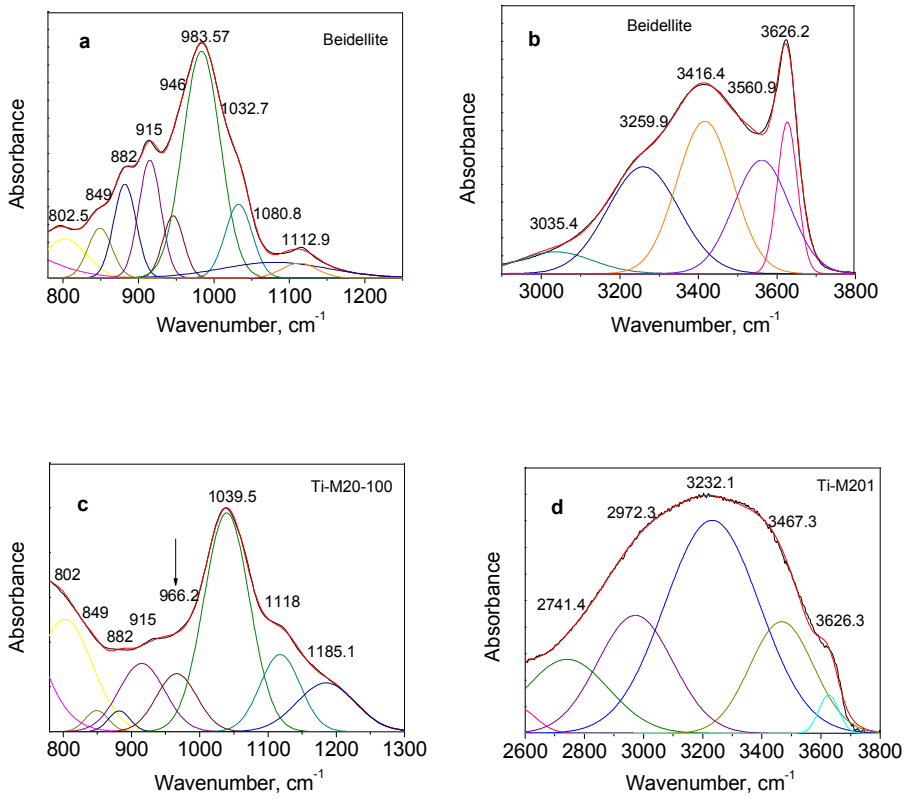

Figure 10. The FTIR bands of the samples. Panel a shows the bands of Beidellite in the range of 800 to 1250 cm^{-1}. and panel b, the bands of Beidellite in the range of 2900 to 3800 cm^{-1}. Panel c shows the FTIR bands in the range of 800 to 1300 cm^{-}_{1} for Ti-M20-100, and Panel d, the band in the range of 2600 to 3800 cm^{-1} for Ti-M20-100.

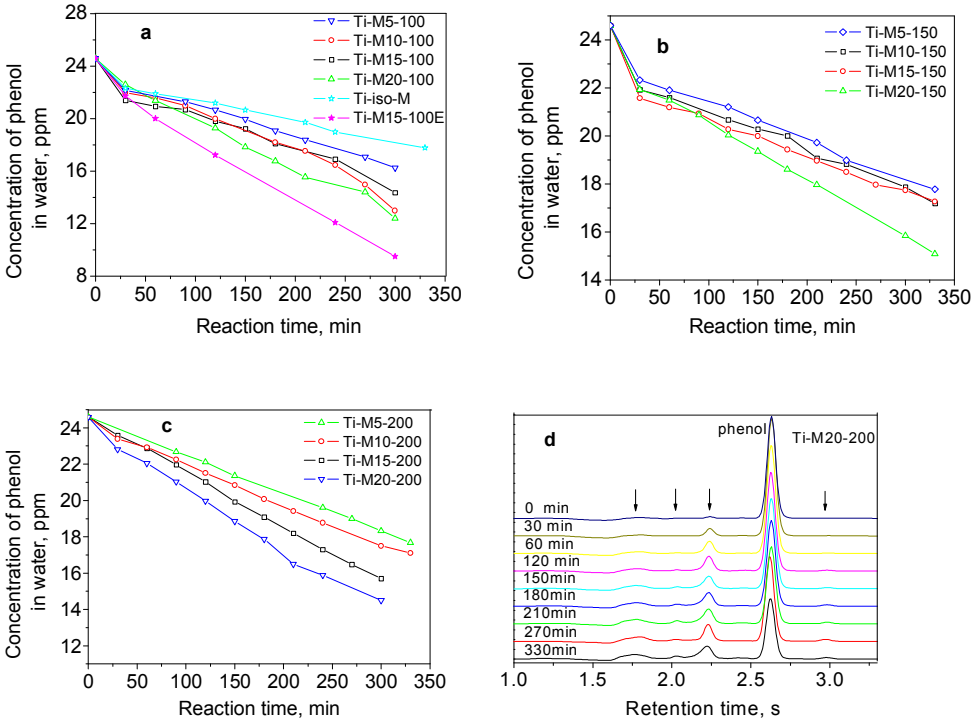

Figure 11. The activity of the samples for degradation of phenol under UV irradiation. Panle a is for the catalysts prepared by the hydrothermal temperature at 100ºC; Panel b is for the catalysts prepared 150ºC and Panel c for the catalysts prepared at 200ºC. The HPLC results of the specimens taken from the reaction system using Ti-M20-100 as the catalyst are given in Panel d, indicating the existence of intermediate.

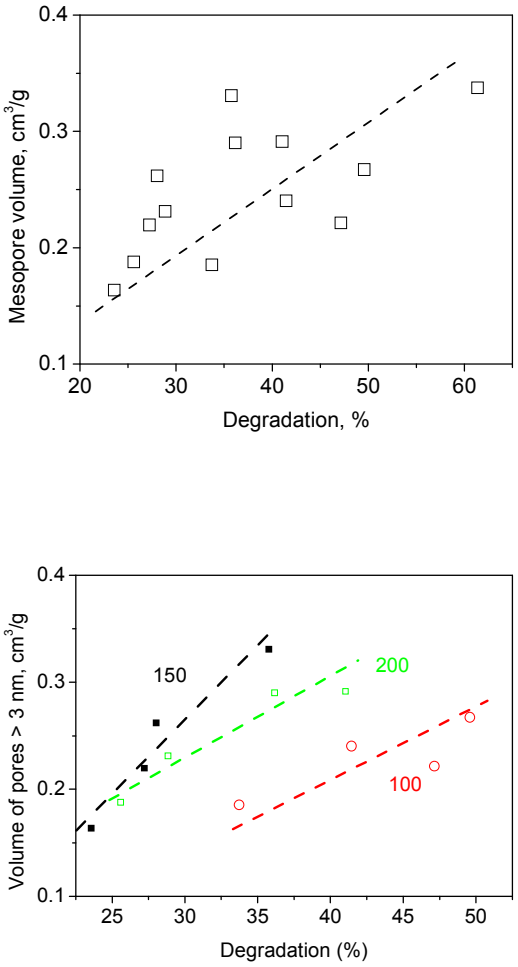

Figure 12 The relation between the catalytic activity and pore volume of the samples (The reaction time is 300min). Top: the relation between the catalytic activity and the mesopore volume for all samples. Bottom: the relation between the catalytic activity and the volume of the pores large than 3 nm, classified in three groups according to the hydrothermal temperature.